

# Asymmetric Surface Brightness Distribution of Altair Observed with the Navy Prototype Optical Interferometer

Naoko Ohishi<sup>1</sup>

*National Astronomical Observatory of Japan, 2-21-1 Osawa, Mitaka, Tokyo 181-8588, Japan*  
naoko.ohishi@nao.ac.jp

Tyler E. Nordgren

*Department of Physics, University of Redlands, 1200 East Colton Avenue, Redlands, CA 92373*  
and

Donald J. Hutter

*U. S. Naval Observatory, Flagstaff Station, P. O. Box 1149, Flagstaff, AZ 86002-1149*

## ABSTRACT

An asymmetric surface brightness distribution of the rapidly rotating A7IV-V star, Altair, has been measured by the Navy Prototype Optical Interferometer (NPOI). The observations were recorded simultaneously using a triangle of three long baselines of 30m, 37m, and 64m, on 19 spectral channels, covering the wavelength range of 520nm to 850nm. The outstanding characteristics of these observations are (a) high resolution with the minimum fringe spacing of 1.7mas, easily resolving the 3-milliarcsecond (mas) stellar disk, and (b) the measurement of closure phase which is a sensitive indicator to the asymmetry of the brightness distribution of the source. Uniform disk diameters fit to the measured squared visibility amplitudes confirms the Altair's oblate shape due to its rapid rotation. The measured observables of Altair showed two features which are inconsistent with both the uniform-disk and limb-darkened disk models, while the measured observable of the comparison star, Vega, are consistent with the limb-darkened disk model. The first feature is that measured squared visibility amplitudes at the first minimum do not reach 0.0 but rather remain at  $\approx 0.02$ , indicating the existence of a small bright region on the stellar disk. The other is that the measured closure phases show non-zero/180 degrees at all spectral channels, which requires an asymmetric surface brightness distribution. We fitted the measured observables to a model with a bright spot on a limb-darkened disk and found the observations are well reproduced by a bright spot, which has relative intensity of 4.7%, on a 3.38 mas limb-darkened stellar disk. Rapid rotation of Altair indicates that this bright region is a pole, which is brighter than other part of the star owing to gravity darkening.

*Subject headings:* techniques: high angular resolution — techniques: interferometric — stars: individual (Altair) — stars: rotation

## 1. Introduction

The impact of stellar rotation upon fundamental stellar parameters was originally calculated by von Zeipel (von Zeipel 1924). He showed that the stellar radius and the surface brightness are ex-

pressed as a function of the latitude; the radius increases and the brightness decreases from the pole to the equator. The first attempt to determine the stellar oblateness owing to rapid rotation was performed with the intensity interfer-

ometer at Narrabri (Hanbury Brown et al. 1967). Though they mentioned the possibility of a rotationally flattened shape for Altair, their data was insufficient to decide the oblateness critically. In 2001, van Belle et al (2001) observed Altair using two baselines of the Palomar Testbed Interferometer (PTI, Colavita et al. 1999). They calculated the apparent stellar angular diameters from measured squared visibility amplitudes using the uniform-disk model and found that the angular diameters change with position angle. This was the first measurement of stellar oblateness owing to rapid rotation. They evaluated the effect of surface brightness distribution caused by gravity darkening on their angular diameter data. Because their simulation showed that the diameters are changed only a few %, they neglected the gravity darkening effect. In 2003, a large oblateness of the Be star Achernar was measured with the VLTI (Domiciano de Souza et al. 2003). They analyzed measured deformation with Roche model which takes the surface brightness distribution owing to gravity darkening into account, but the deformation was too large to be explained within the range of the model. Though both the measurement at PTI and VLTI demonstrated the determination of the stellar parameters such as orientation of the rotation axis and the apparent oblateness from the squared visibility amplitudes obtained with the interferometer, the effect of surface brightness distribution was not determined.

Because of the rapid rotation of Altair, where apparent rotational velocities range from  $v \sin i = 190 \text{ km/s}$  (Carpenter et al. 1984) to  $250 \text{ km/s}$  (Stoeckley 1968), this star is expected to be gravity darkened. However, the effects of the stellar surface brightness distribution on squared visibility amplitudes are small at low-resolution before the first minimum. For example, the effect of limb darkening on visibilities becomes more significant after the first minimum. Consequently, in order to discuss the surface brightness distribution of rapidly rotating stars, it is indispensable to have high-resolution measurements at least over the first minimum. In 2001, the NPOI achieved an array configuration (see next section) which for the first time allowed for observations with a baseline as long as 64 m. With this long baseline and visible observing wavelength, the minimum fringe spacing becomes as small as 1.7 mas at the sky

position of Altair. This resolution is high enough to observe this  $\approx 3$  mas star well over the first minimum. Moreover, the NPOI is equipped with a system which enables measurement of closure phase in addition to the squared visibility amplitudes since 1996 (Benson et al. 1997). Closure phase is a sensitive measure to the asymmetry of the brightness distribution of a source. If the gravity darkened stellar disk is seen neither equator on nor pole on, the intensity distribution of the source projected on a baseline will be asymmetric and we expect that the measurement of the closure phase gives us useful information about inclination of the star. Consequently, we expect that observations of Altair with the NPOI will provide better information than earlier observations in order to examine the surface brightness distribution of this rapidly rotating star.

Observations are done for four nights from 25 May to 1 June in 2001 using three baselines of 30 m, 37 m, and 64 m of NPOI. We examine the apparent stellar diameters reduced using a uniform-disk model, and discuss the surface brightness distribution of this star.

## 2. Observations

The NPOI, located near Flagstaff, AZ, is a long-baseline optical interferometer which consists of an astrometric subarray (four elements) and an imaging subarray (six elements) (Armstrong et al. 1998). For each baseline, data are collected in thirty-two spectral channels cover the observing wavelength from 450nm to 850nm. We used three baselines consisting of three siderostats; two of which were in astrometric subarray, AW, AE, and one of which was in imaging subarray, W7. In this paper, we state each baseline as follows: OB1(AW-AE), OB2(W7-AW), and OB3(AE-W7). The arrangement and the length of each baseline is shown in Tab. 1.

We observed Altair for four nights from 25-27 May, and 1 June in 2001 and obtained 19 scans (Hummel et al. 1998) of data. Detailed observation table is shown in Tab. 2. Interposed with the observations of Altair were observations of the calibration star,  $\zeta$  Aql, and a comparison star  $\alpha$  Lyr, Vega. We chose Vega as a comparison star because of its similar spectral type, magnitude, and angular size to that of Altair. In addition,

TABLE 1  
ARRANGEMENT OF THREE BASELINES USED FOR OBSERVATION.

baseline	station	E [m]	N [m]	Z [m]	length [m]
OB1	AW-AE	-37.379245	-2.60124	0.000314	37.46964647
OB2	W7-AW	-23.813216	-17.49076	-0.080794	29.54661519
OB3	AE-W7	61.192461	20.092	0.08048	64.40661631

Table 2: Observation table for Altair.

date	scan no.	Hour Angle [hr]	OB1		OB2		OB3	
			P. A. [deg]	UDD [mas]	P. A. [deg]	UDD [mas]	P. A. [deg]	UDD [mas]
May25	Pt 81	-0.470	182.5	3.10	211.6	3.23	195.2	3.16
	Pt 84	-0.318	182.8	3.01	212.1	3.16	195.6	3.18
	Pt 87	-0.167	183.2	2.99	212.7	3.12	196.0	3.20
	Pt 90	-0.017	183.5	2.97	213.4	3.09	196.4	3.19
	Pt 93	0.132	183.9	3.08	214.1	3.17	196.8	3.15
	Pt 97	0.629	185.1	3.14	216.7	3.44	198.5	3.18
	Pt 100	0.827	185.6	3.16	218.0	3.32	199.3	3.18
May26	Pt 30	-0.242	183.0	3.04	212.4	3.20	195.8	3.17
	Pt 35	0.208	184.1	2.91	214.4	3.13	197.1	3.18
	Pt 38	0.775	185.5	3.20	217.6	3.44	199.1	3.19
May27	Pt 23	-0.967	181.4	3.15	210.0	3.25	194.1	3.17
	Pt 30	-0.484	182.5	3.14	211.5	3.25	195.2	3.14
	Pt 35	-0.146	183.2	3.03	212.8	3.18	196.0	3.21
	Pt 39	0.142	183.9	3.08	214.1	3.28	196.9	3.18
	Pt 44	0.475	184.7	3.27	215.8	3.54	198.0	3.17
Jun01	Pt 14	-1.041	181.2	3.18	209.8	3.26	194.0	3.12
	Pt 19	-0.726	181.9	3.09	210.7	3.31	194.6	3.15
	Pt 24	-0.410	182.6	3.06	211.8	3.23	195.3	3.17
	Pt 29	-0.120	183.3	3.03	212.9	3.23	196.1	3.16

<sup>a</sup>Position Angle, P. A., is east of north. For OB3, 180 degree are added. UDD is uniform disk diameter.

Vega is a good comparison when we discuss the oblateness of Altair because we expect negligible deformation from a circularly symmetric disk given that its observed rotational velocity is less than 20km/s (Freire Ferrero et al. 1983). During our observations, the measured squared visibility amplitudes of Vega showed dependence on zenith angle when the star passed within 10 degrees of zenith. No such dependence was found outside this region. Consequently, we removed data of Vega with zenith angle smaller than 10 degree. Fourteen scans of Vega remained after this selection. We used all 19 scans of Altair because that star doesn't pass the region close to the zenith. We also used all data of  $\zeta$  Aql and the number of scans of this star during four nights was 24.

$\zeta$  Aql was used to calibrate measured observables of both Altair and Vega. The uniform disk diameter of this calibration star is computed as 0.80mas from its observed color and magnitude (Mozurkewich et al. 1991). This value is also used in other observation (Nordgren et al. 1999). Though the size of the star, 0.80mas, is small compared with Vega and Altair, the star is partly resolved with the longest baseline; measured with the full 64.4m baseline, squared visibility amplitudes become about 0.7 for a perfect interferometer. Because  $\zeta$  Aql is a rapidly rotating star with  $v \sin i \sim 320\text{km/s}$  (Royer et al. 2002), we examined the possibility that using this star as a circular disk with the diameter of 0.80mas biases the results of Vega and Altair. We evaluated the effect of rotation as 5% changes in diameter and 5% asymmetric brightness distribution on the star owing to gravity darkening. At the longest baseline, we found that these features change the squared visibility amplitudes about 6% and phase about 3 degree at most. The calculated possible errors of squared visibility amplitudes and phase were almost the same level with the measurement errors, which are described in sec. 2.2. Consequently, the effect of the rapid rotation of the calibration star is not critical to our result, but we need to be careful when we reduce precise physical parameters directly from measured observables.

Because the signal to noise ratio of the measured visibilities decreases as the wavelength becomes shorter, we used only the 20 reddest of the 32 spectral channels, thus covering wavelengths from 520nm to 850nm. The raw squared visibil-

ity amplitudes of the calibration star depend on channels and baselines. The highest raw  $V^2$  was  $0.71 \pm 0.04$  at the reddest channel of OB2 ( $V^2$  for a perfect interferometer on a 0.8mas star is 0.96) and the lowest raw  $V^2$  was  $0.13 \pm 0.01$  at the bluest channel of OB3 ( $V^2$  for a perfect interferometer on a 0.8mas star is 0.6). We also removed the data obtained at the spectral channel with wavelength,  $\lambda = 633\text{nm}$ , because this channel contains light from the NPOI's He-Ne metrology laser. One detector for OB3 was not available during our observations and one other one didn't work on 1st June 2001. Consequently, the number of data were, 19 spectral channels  $\times$  19 scans=361 squared visibility amplitudes on OB1 and OB2, 18 spectral channels  $\times$  15 scans + 17 spectral channels  $\times$  4 scans = 338 squared visibility amplitudes on OB3, triple amplitudes, and closure phases. The total number of data were  $361 \times 2 + 338 \times 3 = 1,738$ .

## 2.1. Detector dead time correction

Before calibrating the measured observables, we corrected the effect of detector dead time. When we observe bright stars such as Altair and Vega, the effect of detector deadtime  $t_d$  is not negligible. The deadtime of the detectors, which are used at the NPOI, are approximately 200ns. The number of photons counted per unit cycle (500Hz) at the detectors of the red spectral channels become about 800; one photon is detected per approximately  $2.5 \mu$  sec. In such case, the number of photons counted at the detectors becomes less than the number of incident photons, and the response of the detector becomes non-linear. This is a well known effect and we calculate the actual photon count rate,  $CR_a$ , using measured photon count rate,  $CR_m$ , as follows,

$$CR_a = \frac{CR_m}{1 - t_d CR_m}. \quad (1)$$

Here, count rate is the number of photons counted per one second.

We calculated the actual visibility  $|V_a|$  using the measured visibility  $|V_m|$  as follows,

$$|V_a| = \frac{|V_m|}{1 - t_d CR_m \times (1 - |V_m|^2)}. \quad (2)$$

This correction changed the squared visibility amplitudes of Vega up to 20%. In this paper, we treat

the detector deadtime correction as described above. Triple amplitudes are also corrected based on eq. (2).

## 2.2. Measurement errors

The statistical errors of measured quantities are calculated and recorded for each scan. However, actual measurement errors are sometimes dominated by long-term errors rather than statistical errors within short-term measurement (Wittkowski et al. 2001). Generally, it is not easy to evaluate long-term systematic errors. In this paper, we calculated the variance of calibrated quantities,  $\sigma_{\text{cal}}(\lambda_j)$ , of the calibration star as long-term errors and estimated errors of measured squared visibility amplitudes,  $\sigma_{\text{vs}}(t_i, \lambda_j)$ , as follows,

$$\sigma_{\text{vs}}^2(t_i, \lambda_j) = \sigma_{\text{vs,stat}}^2(t_i, \lambda_j) + \sigma_{\text{vs,cal}}^2(\lambda_j) \times \frac{|V(t_i, \lambda_j)|^2}{\sum_{i=0}^{N-1} |V_{\text{cal}}(t_i, \lambda_j)|^2 / N}. \quad (3)$$

Here,  $t_i$  is the time at the  $i$ -th scan,  $\lambda_j$  is the wavelength at the  $j$ -th spectral channel,  $\sigma_{\text{vs,stat}}(t_i, \lambda_j)$  is the statistical error,  $|V(t_i, \lambda_j)|^2$  is the calibrated squared visibility amplitudes of the source,  $|V_{\text{cal}}(t_i, \lambda_j)|^2$  is the calibrated squared visibility amplitudes of the calibration star, and  $N$  is the number of scans. We also estimated measurement errors of triple amplitudes as above. For closure phases, we used the following equation,

$$\sigma_{\text{cp}}^2(t_i, \lambda_j) = \sigma_{\text{cp,stat}}^2(t_i, \lambda_j) + \sigma_{\text{cp,cal}}^2(\lambda). \quad (4)$$

The ratio of errors calculated using eqs. (3), and (4) to the statistical errors were 4.8 (for squared visibility amplitudes at OB1), 15.4 (OB2), 1.4 (OB3), 2.7 (for triple amplitudes), 1.1 (closure phases). This means that the measurement errors of these observations are nearly dominated by the long-term errors rather than short-term statistical errors. Even if the measurement errors are dominated by long-term errors, it is confirmed that data obtained at NPOI shows no systematic error compared with data obtained at other interferometer (Nordgren, Sudol, and Mozurkewich 2001).

## 3. Results

The squared visibility amplitudes on three baselines, triple amplitudes, and closure phases on

about 19 channels were obtained simultaneously for each scan in our observation. Visibility measured at a baseline with projected baseline,  $B_p$ , of a stellar interferometer, which is the Fourier transform of the brightness distribution of the source, is written as follows,

$$V(kB_p) = \frac{\int I(x) \exp[-ikB_p x] dx}{\int I(x) dx}, \quad (5)$$

where  $I(x)$  is the brightness distribution projected to the baseline,  $k = 2\pi/\lambda$  is the wavenumber. For example, visibility of the uniform-disk with the angular radius of  $r_{\text{UD}}$  is written as follows,

$$V_{\text{UD}}(r_{\text{UD}}) = \frac{2J_1(kB_p r_{\text{UD}})}{kB_p r_{\text{UD}}}. \quad (6)$$

Visibility of the limb-darkened disk with the angular radius of  $r_{\text{LD}}$  and the linear limb darkening coefficient of  $u(k)$  is written as follows (Quirrenbach et al. 1996),

$$V_{\text{LD}}(r_{\text{LD}}) = \frac{6}{3-u(k)} \{1-u(k)\} \frac{2J_1(kB_p r_{\text{LD}})}{kB_p r_{\text{LD}}} + \frac{6}{3-u(k)} u(k) \sqrt{\frac{\pi}{2}} \frac{J_{3/2}(kB_p r_{\text{LD}})}{(kB_p r_{\text{LD}})^{3/2}}. \quad (7)$$

The triple product is the product of the visibilities on three baselines that form a triangle,

$$V_{\text{TP}} = |V_1| \exp(-i\Phi_1) |V_2| \exp(-i\Phi_2) |V_3| \exp(-i\Phi_3). \quad (8)$$

The triple amplitude is the absolute value of the triple product,

$$|V_{\text{TP}}| = |V_1| |V_2| |V_3|, \quad (9)$$

and the closure phase is the phase of the triple product,

$$\Phi_c = \Phi_1 + \Phi_2 + \Phi_3. \quad (10)$$

As we can see from eq. (5), if the brightness distribution of the source projected to a baseline,  $I(x)$ , is symmetric with  $x$ , the imaginary part of the visibility is zero and the phase of the visibility takes 0 or  $\pm 180$  degree. If the brightness distribution of the source is asymmetric, the imaginary part of the visibility becomes non-zero and the phase takes non-zero/ $\pm 180$  degree. Generally, it is not easy to measure phase of visibility with a ground interferometer because of atmospheric turbulence.

However, the closure phase cancels the effect of atmospheric turbulence and conserves information of the source. Consequently, closure phase is a useful interferometric observable in order to discuss asymmetry of brightness distribution of the source.

### 3.1. Measured squared visibility amplitudes, triple amplitudes, and closure phases

Vega was chosen as a comparison star due to its similarities in size, spectral type, and magnitude with Altair, but yet without the high observed rotational velocity which would lead to apparent oblateness. Figure 1 shows the squared visibility amplitudes and triple products measured during the night of 25 May 2001 for Vega. Figure 2 shows the observables of Altair measured on the same night. The dashed lines show the uniform-disk model with the fitted angular diameters of  $2r_{\text{UD}} = 3.17\text{mas}$  for Altair, and  $2r_{\text{UD}} = 3.11\text{mas}$  for Vega. The solid lines show the limb-darkened disk model with the fitted angular diameters of  $2r_{\text{LD}} = 3.32\text{mas}$  for Altair and  $2r_{\text{LD}} = 3.22\text{mas}$  for Vega. In order to calculate the limb darkening model, we used linear limb darkening coefficients calculated by van Hamme (Van Hamme 1993) with parameters,  $T_{\text{eff}}=7750\text{K}$  and  $\log g=4.0$  for Altair, and  $T_{\text{eff}}=9500\text{K}$  and  $\log g=4.0$  for Vega.

The measured observables of Vega are better fitted with the limb-darkened model (reduced  $\chi^2 = 7.5$ ), than with the uniform-disk model (reduced  $\chi^2 = 17.2$ ). The limb-darkened disk diameter of Vega measured at PTI was  $3.28 \pm 0.01\text{mas}$  (Ciardi et al. 2001) and the diameters are consistent with about 2% error. However, Altair was not well fitted with either the uniform-disk model (reduced  $\chi^2 = 150$ ) or the limb-darkened model (reduced  $\chi^2 = 154$ ). Altair’s large inconsistency between the measured observables and models is mainly owing to the facts that: (a) the squared visibility amplitudes at OB3 and the triple amplitudes around the first minimum do not decrease to zero, and (b) the closure phases show non-zero/180 degree at all spectral channels. In addition, the measured squared visibility amplitudes at OB1 are slightly bigger than the circular uniform disk model while that at OB2 is slightly smaller than the model. The discrepancy of measured squared visibility amplitudes and triple am-

plitudes from the model around the first minimum indicates that there is a small bright component on the stellar disk, which is not resolved even with the longest baseline. Non-zero/180 degree of closure phases means the brightness distribution of the source is asymmetric.

### 3.2. Apparent Stellar Diameters Reduced from the Uniform Disk Model

Before considering the discrepancy from the uniform-disk model, we first examine whether the uniform disk angular diameter reduced from the squared visibility amplitudes changes with position angle and whether the change is consistent with the PTI result. We consider the diameter change assuming the elliptical shape of the stellar disk. The brightness distribution of a uniform ellipse projected to a baseline with position angle  $\phi$  becomes the same with that of the circular uniform-disk with angular radius,  $r(\phi)$ ,

$$r(\phi) = \sqrt{a^2 \sin^2(\phi - \phi_0) + b^2 \cos^2(\phi - \phi_0)}, \quad (11)$$

where  $a$  is the angular radius at the major axis,  $b$  is the angular radius at the minor axis, and  $\phi_0$  is the orientation angle of the ellipse on the sky, where  $\phi_0 = 0$  corresponds to the minor axis pointing to the north on the sky. As a result, the squared visibility amplitude becomes the same as that of eq. (6) with the angular radius,  $r(\phi)$ . Consequently, in order to determine the parameters of the ellipse, we reduce the data using the following procedure: first, calculate the angular diameters at a position angle by fitting the squared visibility of each scan at each baseline with eq. (6), then compare the reduced diameters with eq. (11). Notice  $r(\phi)$  is a little different from the intercept of an ellipse at an angle  $\phi$ .

Though the errors of fitted angular diameters are calculated from the errors of visibilities, we found that the scatters of the diameters were a few times larger than the calculated errors at OB1 and OB2. Thus we define the errors of the fitted angular diameters in another way. Considering the small change of position angle at each baseline,  $4^\circ$  (OB1),  $5^\circ$  (OB2),  $8^\circ$  (OB3) (Tab. 2) during the observation, we regard the change in angular diameter of the ellipse with position angle as small compared to the scatter of the fitted angular diameters. We therefore used the variance of the

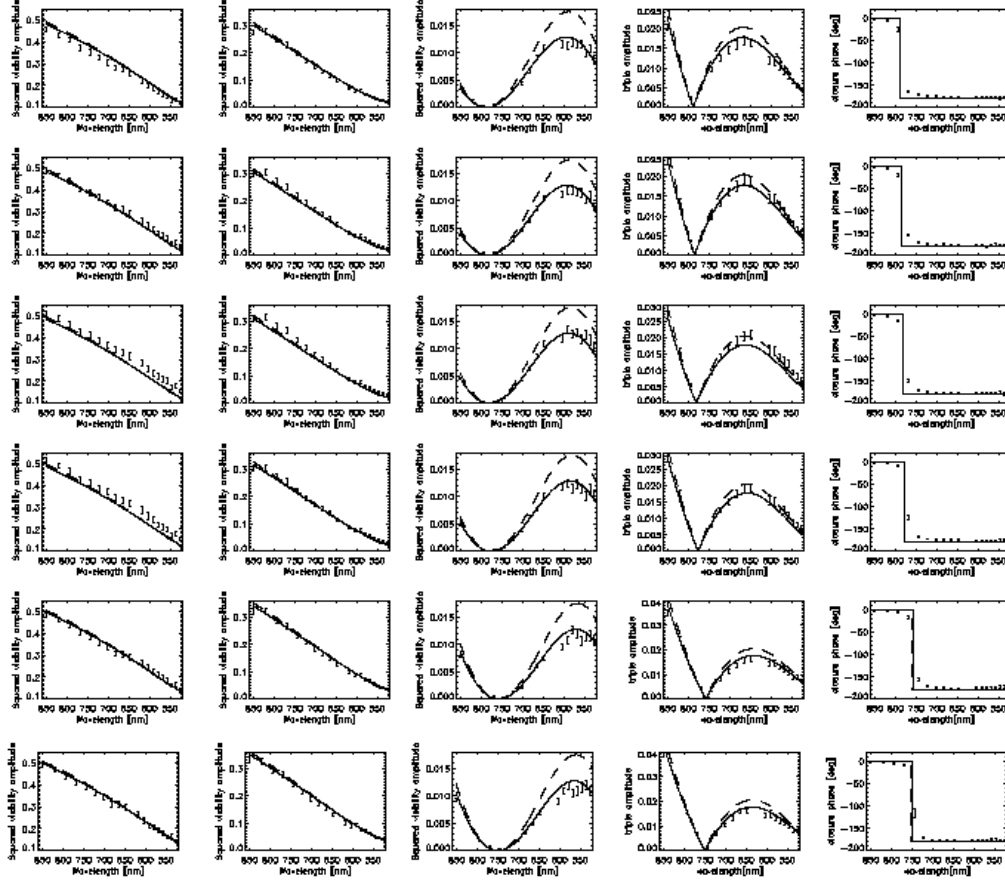


Fig. 1.— From left to right, squared visibility amplitudes on OB2, OB1, and OB3, triple amplitudes, and closure phases of Vega measured during 25 May 2001. Six scans were obtained. Dashed lines show the uniform-disk model with diameter of 3.11mas. Solid lines show the limb-darkening model with diameter of 3.22mas. We used linear limb darkening coefficients calculated by van Hamme, with  $T_{\text{eff}}=9500\text{K}$  and  $\log g=4.0$ . The limb-darkening model reproduces the measured squared visibility amplitudes and triple amplitudes better than the uniform disk model.

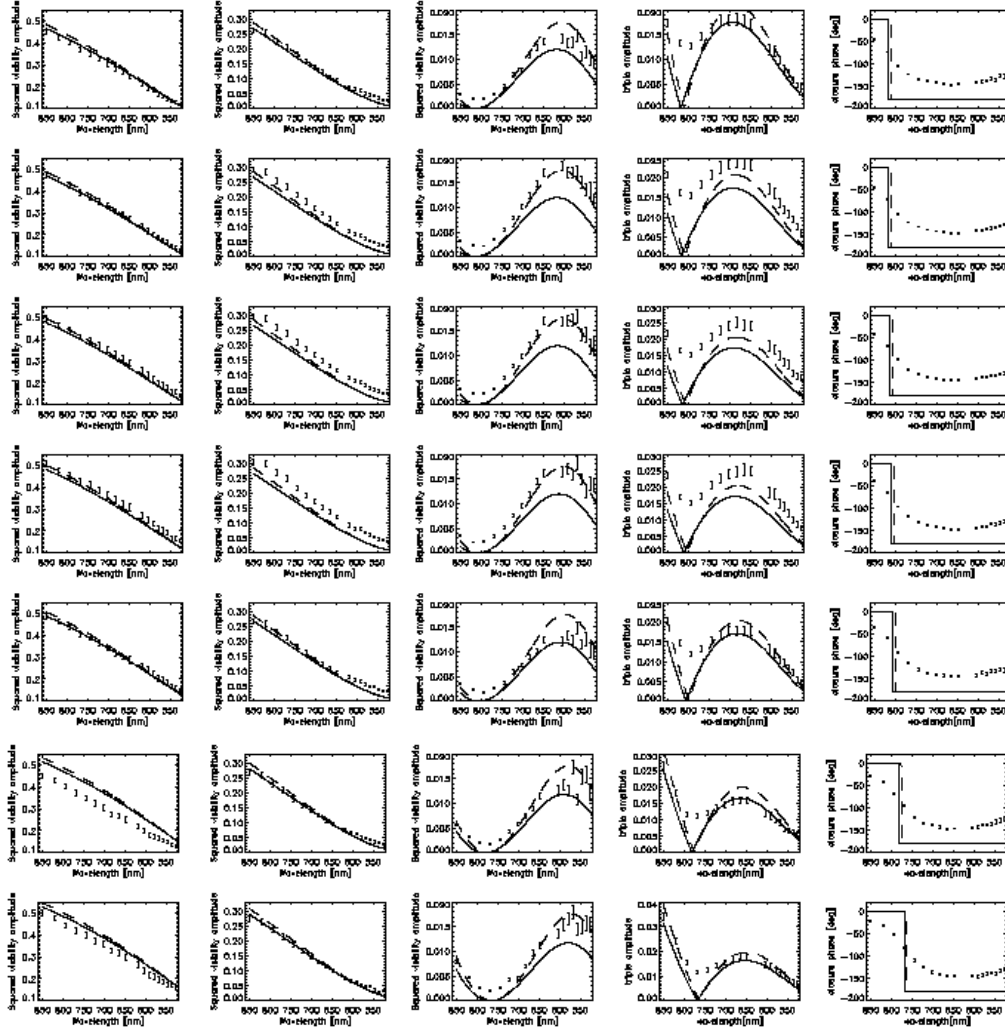


Fig. 2.— From left to right, squared visibility amplitudes at OB2, OB1, and OB3, triple amplitudes and closure phases of Altair measured during the night of 25 May 2001. Seven scans were obtained. Dashed lines show the uniform-disk model with diameter of 3.17mas. Solid lines show the limb-darkening model with diameter of 3.32mas. We used linear limb darkening coefficients calculated by van Hamme, with  $T_{\text{eff}}=7750\text{K}$  and  $\log g=4.0$ . It is significant that the squared visibility amplitudes at OB3 and the triple amplitudes around the first minimum don't decrease to zero, and the closure phases show non-zero/180 degree at all spectral channels.



fitted angular diameters at each baseline, 0.09mas (OB1), 0.11mas (OB2), 0.02mas (OB3) as errors of the fitted angular diameters. The error of the fitted angular diameters on OB3 is smaller compared with that of on OB1 and on OB2. We consider this fact is owing to that the measured visibilities cover the first minimum at OB3 and the position of the first minimum improves the precision of the fitted diameters.

Figure 3 shows fitted angular diameters with horizontal axis of position angle. The reduced  $\chi'^2$  of 1.5 calculated based on the scatter of the diameters of Altair, with the circular uniform disk model is improved to 0.95 when we allow the diameter of Altair to change with position angle. Fitted parameters with eq. (11) become  $2a = 3.31 \pm 0.09\text{mas}$ ,  $2b = 2.93 \pm 0.17\text{mas}$ ,  $\phi_0 = 35^\circ \pm 18^\circ$ . In our case, the uniform disk model estimates the angular diameters of Altair about 0.14mas smaller than the limb-darkening model. Resultant parameters corrected for the limb darkening effect are consistent with the PTI result (van Belle et al. 2001),  $2a = 3.461 \pm 0.038\text{mas}$ ,  $2b = 3.037 \pm 0.069\text{mas}$ ,  $\alpha_0 = 25^\circ \pm 9^\circ$ . Compared with Altair, fitted diameters and errors calculated from the scatters of the fitted diameters on each baseline of Vega are shown in Fig. 3. The diameter fitted with the circular uniform-disk model was,  $2r_{\text{UD}} = 3.11 \pm 0.01\text{mas}$ ,  $\chi'^2 = 1.0$  and the value of  $\chi'^2$  was not changed when we used the elliptical model. We found that Altair is well explained by the ellipse rather than the circular disk while Vega is well explained as the circular disk. The dependence of fitted diameters of Altair on the position angle was similar to PTI's.

### 3.3. A small bright region on the limb darkening disk

In this section, we examine whether the two features of measured observables of Altair which are inconsistent with both the uniform-disk and the limb-darkened disk models are reproduced with the model of a single bright region on the limb-darkened disk. When a bright spot with relative intensity of  $I_p$  was located at  $(r_p, \phi_p)$  in polar coordinate on a limb-darkening disk with angular radius of  $r_s$ , visibility is written as follows,

$$V_{\text{model}}(I_p, r_s, r_p, \phi_p) = (1 - I_p)V_{\text{LD}}(r_s) + I_p \exp\{-ikB_p r_p \cos(\phi - \phi_p)\}, \quad (12)$$

With this model, the visibility amplitude at the first minimum becomes  $I_p$ . We can see the value of squared visibility amplitudes around the first minimum about 0.02 and expect that  $I_p = 0.04 \sim 0.05$ . Though the existence of bright spot changes stellar diameter  $2r_s$ , we expect that the change of  $2r_s$  from  $2r_{\text{LD}}=3.32\text{mas}$  is small. We searched the optimal position of the spot ( $r_p$ ;  $0 \sim r_s$ ,  $\Delta r_p=0.01r_s$ ,  $\phi_p$ ;  $0 \sim 360$ ,  $\Delta\phi=1$  [deg]) for each set of  $(I_p, 2r_s)$  ranging ( $I_p$ ; 0.034~0.06,  $2r_s$ ; 3.25~3.51mas). As a result, we found that the set of parameters, ( $I_p=0.047$ ,  $r_s=3.38\text{mas}$ ) gives the best  $\chi_c^2$  of 7.3. The  $\chi^2$  value of 7.3 means that this model reproduces the measured observables at the same level as the limb-darkening model reproduced for Vega. Compared with the oblateness improved  $\chi'^2$  from 1.5 to 0.95, a spot on the circular limb darkened disk improved  $\chi^2$  from 150 to 7.3. It means that the surface brightness distribution is more essential than the oblateness for our data. A spot on the circular limb darkening disk model gave similar  $\chi^2$  of squared visibility amplitudes at OB1 and OB2 to the limb darkened elliptical disk model.

Figure 4 shows the  $\chi^2$  map of  $(I_p, 2r_s)$  and the  $\chi^2$  map of  $(r_p, \phi_p)$  at ( $I_p=0.047$ ,  $2r_s=3.38\text{mas}$ ). Though the parameters  $(I_p, 2r_s)$  converge,  $r_p$  and  $\phi_p$  are not determined independently. These two parameters appear in the second term of eq. (12). The equation indicates that small change of position angle at OB3 during the observation make it difficult to determine  $r_p$  and  $\phi_p$  independently. Consequently, measurement of this star with wider range of position angle, or with additional long baseline which is located perpendicular to the OB3, will be needed to determine the position of the bright region accurately.

## 4. Discussion

The measured observables are well reproduced with a bright spot on the circular limb-darkened disk model. Because Altair is a single star (van Belle et al. 2001) and well known as a rapidly rotating star, it is natural to consider this spot is a bright pole of the gravity darkened star. Van Belle et al. (2001) simulated the effect of the gravity darkening as an additional 25% brighter region covering 20% of the surface of the star on the limb-darkened disk. The relative intensity of

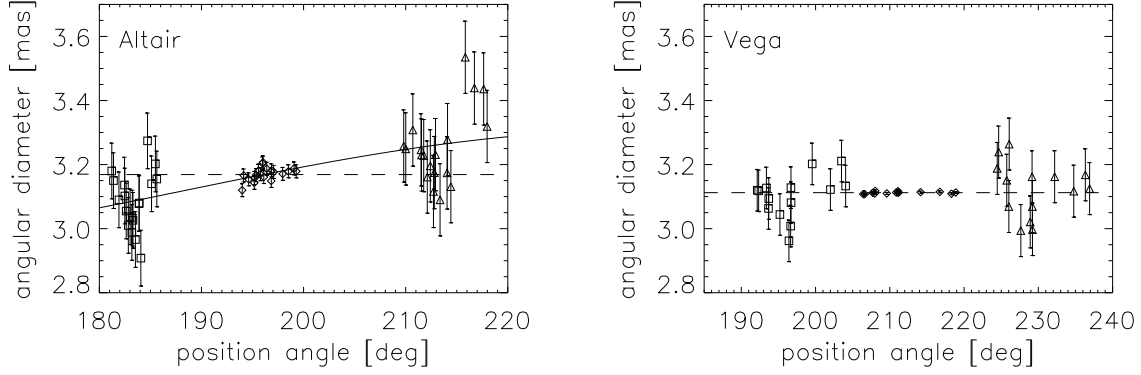


Fig. 3.— Uniform-disk diameters of Altair (left) and Vega (right) as a function of baseline position angle. Squares show fitted angular diameters at OB1, diamonds show fitted angular diameters at OB3, and triangles show fitted angular diameters at OB2. Dashed lines show fitted angular diameters of 3.17mas (Altair) and 3.11mas (Vega). Solid line shows fitted ellipse with parameters of  $2a=3.31\text{mas}$ ,  $2b=2.93\text{mas}$ , and  $\phi_0 = 35^\circ \pm 18^\circ$ .

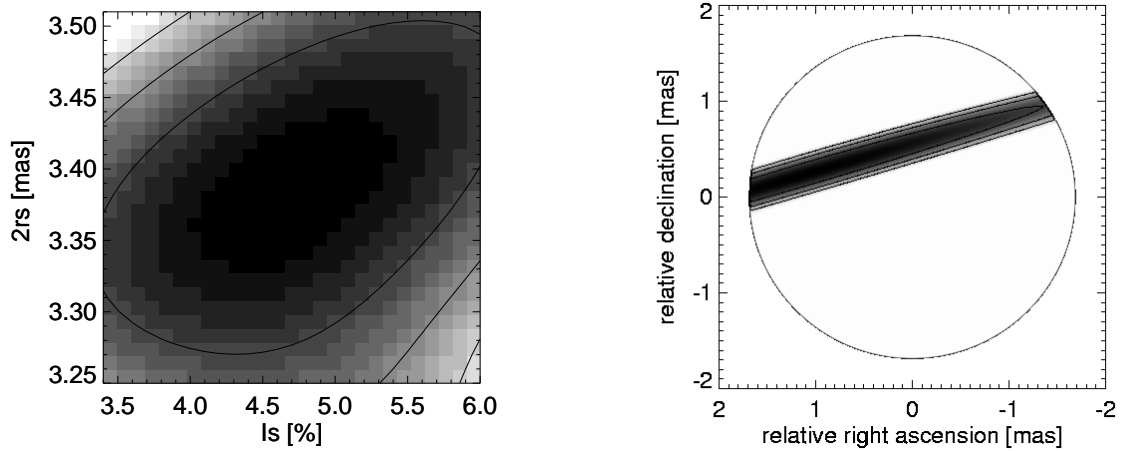


Fig. 4.— Left;  $\chi^2$  map as a function of relative intensity of the bright spot,  $I_p$ , and the limb darkened disk diameter,  $2r_s$ . The minimum value of  $\chi^2$ ,  $\chi_c^2=7.3$ , is given for  $I_p = 4.7\%$  and  $2r_s=3.38\text{mas}$ . Lines show  $2\chi_c^2$ ,  $3\chi_c^2$ , and  $4\chi_c^2$ . Right;  $\chi^2$  map as a function of position of the bright spot,  $(r_p, \phi_p)$ , when parameters,  $I_s=0.047$  and  $2r_s=3.38\text{mas}$ , are given.

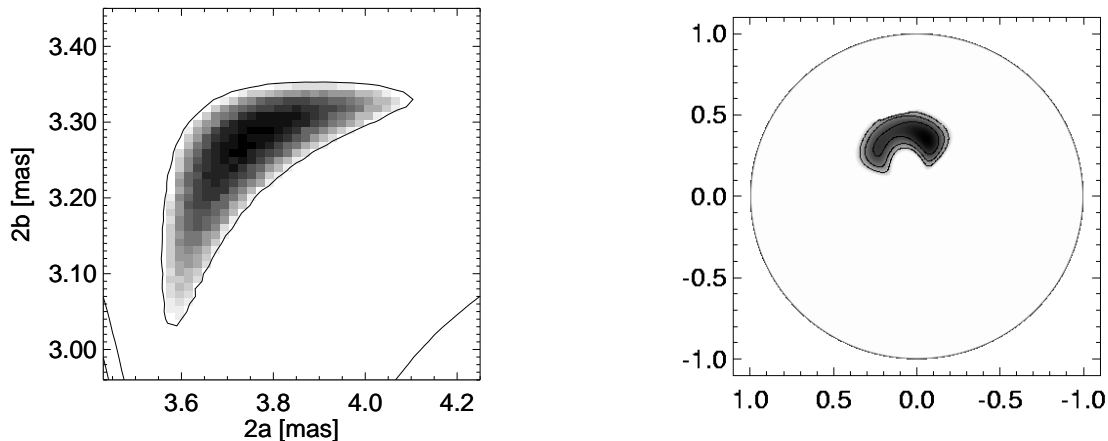


Fig. 5.— Left;  $\chi^2$  map as a function of angular diameters at the major and the minor axes of ellipse,  $2a$ ,  $2b$ . The minimum value of  $\chi^2$ ,  $\chi_e^2=7.0$ , is given for  $2a=3.77\text{mas}$  and  $2b=3.29\text{mas}$ . Lines show  $\chi_c^2$ ,  $2\chi_e^2$ , and  $3\chi_e^2$ . Right;  $\chi^2$  map as a function of position of the bright spot,  $(r_p/b, \phi_p)$ , when parameters  $2a=3.77\text{mas}$  and  $2b=3.29\text{mas}$  are given. Lines show  $2\chi_e^2$ ,  $3\chi_e^2$ , and  $4\chi_e^2$ .

the additional bright region is 5% which is not far off from our result of 4.7%. Considering it as a gravity-darkened star, we expect that it is better to take the effect of oblateness in addition to the surface brightness distribution into account. Then we replaced  $r_s$  in eq. (12) with  $r_{el}(\phi)$ , eq. (11), and fitted measured observables with the model, where a bright spot is on the minor axis of a limb-darkened elliptical disk. Fixing the relative intensity of the spot,  $I_p=0.047$ , we searched the optimized set of  $(r_p/b, \phi_p)$  for each set of  $(2a; 3.43\sim 4.25\text{mas}, \Delta 2a=0.02\text{mas}, 2b; 2.96\sim 3.45\text{mas}, \Delta 2b=0.01\text{mas})$ . We found the minimum  $\chi^2$  decreases only a little to 7.0, which is given with the set of parameters,  $2a=3.77\text{mas}$ , and  $2b=3.29\text{mas}$ . Figure 5 shows the  $\chi^2$  map of  $(2a, 2b)$  and the  $\chi^2$  map of  $(r_p/b, \phi_p)$  at  $(2a=3.77\text{mas}, 2b=3.29\text{mas})$ . It is worth to consider the region where  $(2a, 2b)$  gives smaller  $\chi^2$  than  $\chi_c^2$  because the number of parameters are increased. Two parameters,  $(r_p/b, \phi_p)$ , converge better than in the former model when parameters  $(2a, 2b)$  are given.

Though the decrease of  $\chi^2$  is small, we try to consider physical parameters of this star with the optimized set of parameters of  $2a=3.77\text{mas}$ ,  $2b=3.29\text{mas}$ ,  $r_p/b = 0.36$ ,  $\phi_p = 9^\circ$ . Assuming a rotationally symmetric elliptical stellar body, we can calculate the inclination,  $i = 35^\circ$  using the

equation,

$$\sin i = \sqrt{1 - \frac{b^2}{a^2} \left(1 - \frac{r_p^2}{b^2}\right)}. \quad (13)$$

In this case, the critical velocity of  $v_c=430\text{km/s}$  (Gray 1976) multiplied by  $\sin i=0.58$  becomes  $250\text{km/s}$ . The values  $v \sin i=190\text{km/s}$  (Carpenter et al. 1984),  $250\text{km/s}$  (Stoeckley 1968) determined from spectroscopy are close to but don't break the  $v_c \sin i$ . The apparent brightness distribution with these parameters are shown in Fig. 7.

## 5. Conclusion

We observed Altair with high resolution including the measurement of the triple product using three long baselines of the NPOI for four nights. Measured observables indicate the asymmetric surface brightness distribution of this star; the asymmetry is deduced directly from the definition of the visibility and does not depend on model. Though the measurement of the structure of the surface brightness distribution has been reported for evolved stars (Tuthill, Haniff, and Baldwin 1997), this is the first time that the asymmetric surface brightness distribution for a main sequence star has been found

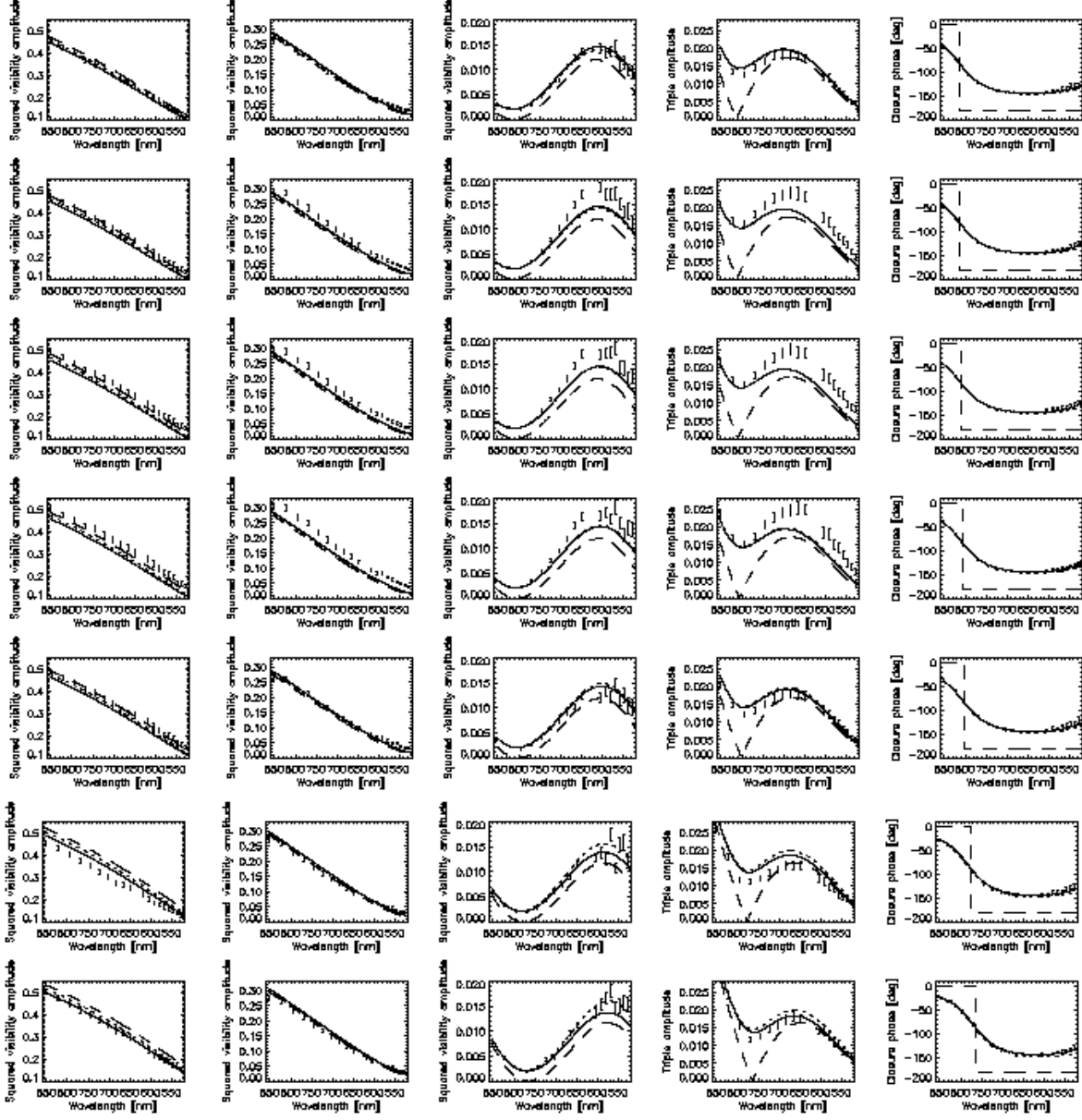


Fig. 6.— Measured observables, squared visibility amplitudes, triple amplitudes and close phases of Altair with models. Solid lines show a spot on the elliptical limb-darkened disk model. Short dashed lines show a spot on the circular limb-darkened disk model. Dashed lines show limb-darkened disk model without spot.

from the direct measurement using interferometry. The measured observables are well reproduced with a model of a bright spot of relative intensity 4.7% on the limb-darkening disk with an angular diameter of 3.38mas. The rapid rotation of the star indicates that the bright spot is a bright pole of gravity-darkened star. Though we couldn't determine the position of the pole owing to insufficient data, we expect that additional observation with sets of long baselines covering wider range of position angle will solve this problem. More sophisticated gravity and limb darkening modeling of a rapidly rotating star (Domiciano de Souza et al. 2002) will also help the determination of physical parameters when we have sufficient multi baselines data. We expect these kinds of observations will be realized with current and future interferometers and that study on rapidly rotating stars will progress with further observation by interferometers.

N. Ohishi acknowledges C. A. Hummel for supporting the use of data reduction system, OYSTER. The Navy Prototype Optical Interferometer is a joint project of the Naval Research Lab and the US Naval Observatory in cooperation with Lowell Observatory, and is funded by the Office of Naval Research and the Oceanographer of the Navy.

## REFERENCES

- Armstrong, J. T., Mozurkewich, D., Rickard, L. J., Hutter, D. J., Benson, J. A., Bowers, P. F., Elias II, N. M., Hummel, C. A., Johnston, K. J., Buscher, D. F., Clark III, J. H., Ha, L., Ling, L. -C., White, N. M., and Simon, R. S. 1998, *ApJ*, 496, 550
- Benson, J. A., Hutter, D. J., Elias II, N. M., Bowers, P. F., Johnston, K. J., Hajian, A. R., Armstrong, J. T., Mozurkewich, D., Pauls, T. A., Rickard, L. J., Hummel, C. A., White, N. M., Black, D., and Denison, C. S. 1997, *AJ*, 114, 1221
- Carpenter, K. G., Slettebak, A., and Sonneborn, G. 1984, *ApJ*, 286, 741
- Ciardi, D. R., van Belle, G. T., Akeson, R. L., Thompson, R. R., Lada, E. A., and Howell, S. B. 2001, *ApJ*, 559, 1147
- Claret, A. 2000, *A&A*, 359, 289
- Colavita, M. M., Wallace, J. K., Hines, B. E., Gursel, Y., Malbet, F., Palmer, D. L., Pan, X. P., Shao, M., Yu, J. W., Boden, A. F., Dumont, P. J., Gubler, J., Koresko, K., Kulkarni, S. R., Lane, B. F., Mobley, D. W., and van Belle, G. T. 1999, *ApJ*, 510, 505
- Domiciano de Souza, A., Vakili, F., Jankov, S., Janot-Pacheco, E., and Abe, L. 2002, *A&A*, 393, 345
- Domiciano de Souza, A., Kervella, P., Jankov, S., Abe, L., Vakili, F., di Folco, E., and Paresce, F. 2003, *A&A*, 407, L47
- Freire Ferrero, R., Gouttebroze, P., Catalano, S., Marilli, E., Bruhweiler, F., Kondo, Y., van der Hucht, K., and Talavera, A. 1983, *ApJ*, 121, 59
- Gray, D. F., 1976, *The Observation and Analysis of Stellar Photospheres* (New York; Wiley-Interscience)
- Hanbury Brown, R., Davis, J., Allen, L. R., and Rome J. M. 1967, *MNRAS*, 137, 393
- Hummel, C. A., Mozurkewich, D., Armstrong, J. T., Hajian, A. R., Elias II, N. M., and Hutter, D. J. 1998, *AJ*, 116, 2536
- Mozurkewich, D., Johnston, K. J., Simon, R. S., Bowers, P. F., and Gaume, R. 1991, *AJ*, 101, 2207
- Nordgren, T. E., Germain, M. E., Benson, J. A., Mozurkewich, D., Sudol, J. J., Elias II, N. M., Hajian, A. R., White, N. M., Hutter, D. J., Johnston, K. J., Gauss, F. S., Armstrong, J. T., Pauls, T. A., and Rickard, L. J. 1999, *AJ*, 118, 3032
- Nordgren, T. E., Sudol, J. J., Mozurkewich, D. 2001, *AJ*, 122, 2707
- Quirrenbach, A., Mozurkewich, D., Buscher, D. F., Hummel, C. A., and Armstrong, J. T. 1996, *A&A*, 312, 160
- Royer, F., Grenier, S., Baylac, M.-O., Gomez, A. E., and Zorec, J. 2002, *A&A*, 393, 897
- Stoeckley, T. R. 1968, *MNRAS*, 140, 121

Tuthill, P. G., Haniff, C. A., and Baldwin, J. E. 1997, MNRAS, 285, 529

von Zeipel, H. 1924, MNRAS, 84, 665

van Belle, G. T., Ciardi, D. R., Thompson, R. R., Akeson, R. L., and Lada, E. A. 2001, ApJ, 559, 1155

Van Hamme, W. 1993, AJ, 160, 2096

Wittkowski, M., Hummel, C. A., Johnston, K. J., Mozurkewich, D., Hajian, A. R., and White, N. M. 2001, A&A, 377, 981

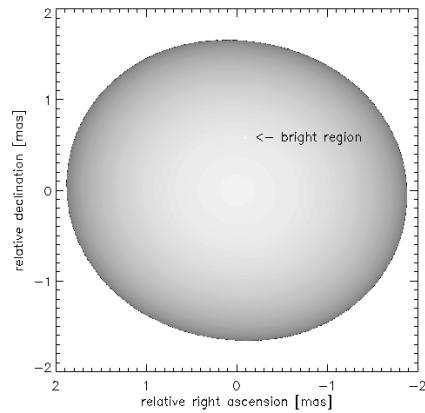


Fig. 7.— A possible solution of a bright spot on the elliptical limb darkening disk model of Altair projected onto the sky with parameters; angular diameter at the major axis  $2a = 3.77\text{mas}$ , angular diameter at the minor axis  $2b = 3.29\text{mas}$ , orientation of the rotational axis projected onto the sky from the north pole  $\phi_0 = 9^\circ$ , relative intensity of the bright spot  $I_p = 4.7\%$ , inclination  $i = 35^\circ$ .